

Cite this: DOI: 10.1039/c0xx00000x

www.rsc.org/xxxxxx

ARTICLE TYPE

Mesoporous Silica Nanoparticles Enhance the Cytotoxicity of Curcumin

Siddharth Jambhrunkar,^{a, ‡} Surajit Karmakar,^{a, ‡} Amiralipi Popat,^a Meihua Yu,^a Chengzhong Yu^a

Received (in XXX, XXX) Xth XXXXXXXXXX 20XX, Accepted Xth XXXXXXXXXX 20XX

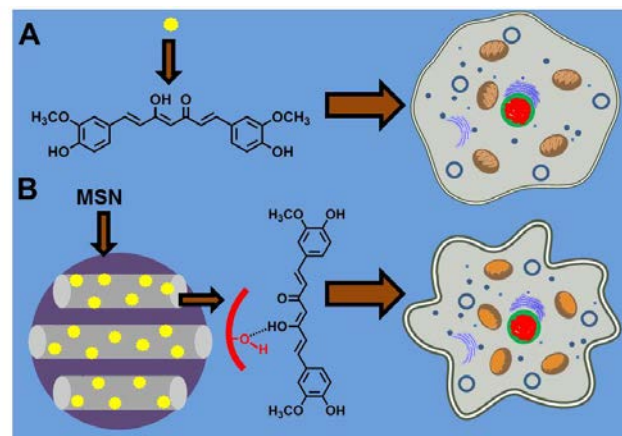
DOI: 10.1039/b000000x

5 **Curcumin encapsulated in mesoporous silica nanoparticles showed improved solubility, *in vitro* release profile and significantly enhanced cell cytotoxicity compared to the pure drug.**

Curcumin, a diferuloylmethane obtained from the rhizomes of the
10 plant *Curcuma longa*,¹ is commonly used as a spice, dye and traditional medicine in Indian and Chinese culture (see Scheme 1A for its structure). Curcumin possesses a range of pharmacological activities such as antiseptic, anti-inflammatory, antioxidant, antiarthritic, and anticancer functions.² It has been
15 found that curcumin inhibits the viability and proliferation in a variety of human cancer cell lines including gastrointestinal cancers, genitourinary cancers, breast cancer, ovarian cancer, lung cancer, melanoma, and sarcoma.^{3, 4} Despite of its advantages, the clinical application of curcumin is stalled due to
20 its poor aqueous solubility leading to poor bioavailability.⁵

Several curcumin delivery systems such as surfactant complex, liposomes, hydrogels, and polymeric nanoparticles have been developed but suffer from synthesis complexity and poor biological stability.⁶⁻⁸ Compared to the organic counterparts,
25 mesoporous silica nanoparticles (MSNs) with rigid inorganic frameworks have attracted increasing attention as drug delivery carriers^{9, 10} owing to their unique properties.¹¹ Previously, curcumin was encapsulated in cetyltrimethylammonium bromide (CTAB) micelle followed by silica coating,¹² or used as a model
30 drug to test its pH-dependent *in vitro* release behavior in modified porous silica materials.^{13,14} It is noted that curcumin undergoes rapid degradation at pH > 7.70 (condition used in *in vitro* release studies).¹⁵ Moreover, CTAB has shown toxicity in cell studies.¹⁶
17 It is concluded that the great potential of MSNs in curcumin
35 formulation, i.e.; using nanopores with high pore volumes as the reservoir for drug loading and controlled release, and using the desired particle size for cellular delivery, is yet to be exploited.

In this work, for the first time, we demonstrate that curcumin can be successfully encapsulated in the nanopores of MSNs
40 through a hydrogen-bonding model (Scheme 1B) leading to significantly higher cell cytotoxicity. Compared to pure drug, the curcumin loaded inside MSNs shows enhanced solubility, sustained release profile, and improved cell cytotoxicity towards SCC-25, a skin cancer cell line. It is shown that the cellular
45 toxicity is associated with the inhibition of polycomb group (PcG) onco-proteins, which are highly expressed in cancer cells and responsible for the cell proliferation and survival.^{18, 19} The curcumin encapsulated in MSNs sufficiently knocks down the



50 **Scheme 1** Schematic representation comparing treatment of SCC-25 cell with pure curcumin (A) and curcumin encapsulated MCM-41 (B) displaying higher cytotoxic effect by curcumin encapsulated MCM-41.

expression level of PcG proteins, thus the growth and
55 transformation of cancer cells are inhibited.²⁰

MCM-41²¹ type MSNs were synthesized and curcumin (CUR) was encapsulated into calcined MCM-41 (MCM-41-CUR) by a simple rotary evaporatory (Rotavap) technique (See Electronic Supplementary Information, ESI). For comparison the physical
60 mixture of MCM-41 and curcumin (MCM-41-CUR PM) was also prepared.

The X-ray diffraction (XRD) pattern of calcined MCM-41 (Fig. S1A) shows three well resolved diffractions at 2θ of 2.68, 4.63 and 5.34° with a reciprocal d-spacing ratio close to 1: $\sqrt{3}$: 2, which can be indexed as 100, 110 and 200 reflections of an ordered two-dimensional (2D) hexagonal mesostructure (p6mm). MCM-41-CUR displayed XRD pattern similar to that of MCM-41 demonstrating retention of the ordered structure after the curcumin encapsulation. Transmission electron microscopy
70 (TEM) image of MCM-41 shows the typical well-ordered hexagonal structure (Fig. S1B) and mean size of 164 nm (PDI=0.23) and 190 nm (PDI=0.31) for MCM-41 and MCM-41-CUR respectively (Fig. S1C).

The N_2 adsorption-desorption isotherms of MCM-41 and
75 MCM-41-CUR (Fig. S2A) exhibited typical type IV isotherm and a steep capillary condensation step occurring at a relative pressure (P/P_0) range of 0.2-0.4. Compared to MCM-41, the surface area and pore volume of MCM-41-CUR decrease (Table S1). From the pore size distribution curves it is shown that the pore size of

MCM-41-CUR decreases from 2.23 to 2.12 nm (Fig. S2B),

indicating that CUR forms nano-sized aggregates in the pores.

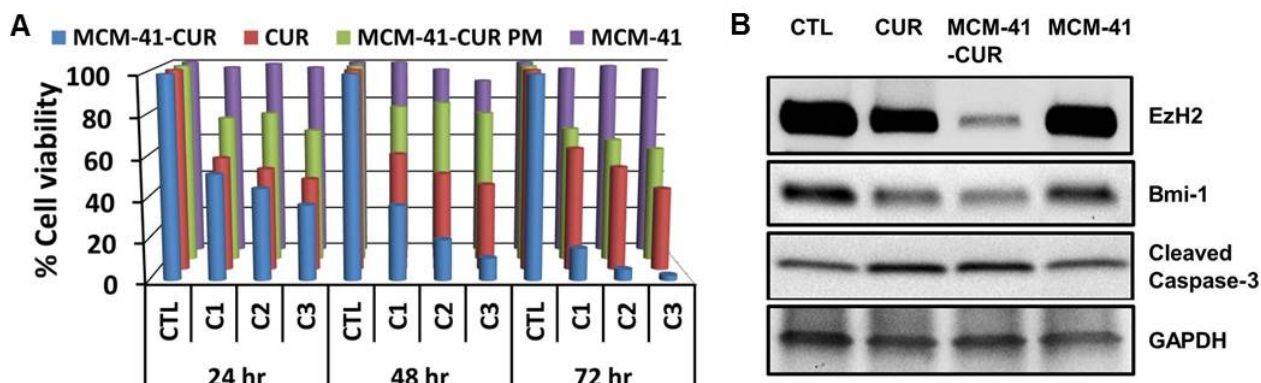


Fig. 1 In vitro cytotoxicity of pure curcumin, MCM-41-CUR and MCM-41-CUR PM in SCC-25 cell line after 24, 48 and 72h (A). CTL, C1, C2 and C3 denote the control group, curcumin equivalent dose of 15 ppm, 30 ppm and 45 ppm respectively used in the cell cytotoxicity experiment. Protein expression studies using Western blot analysis for pure curcumin, MCM-41-CUR and MCM-41 (B).

Thermogravimetric analysis (TGA) shows 17% of curcumin encapsulation for MCM-41-CUR (Fig. S3A), indicating a high efficiency (85%) of the Rotavap process used for curcumin encapsulation, in accordance with a previous report.²² For comparison, MCM-41-CUR PM sample shows a CUR weight loss of 20% identical to the feed ratio in the physical mixing. Differential scanning calorimetry (DSC) analysis was performed to determine the crystallisation behaviour of curcumin in MCM-41-CUR and MCM-41-CUR PM (Fig. S3B). Pure curcumin clearly displays a sharp melting point peak at 176 °C. A small peak is observed for MCM-41-CUR PM indicating existence of curcumin's crystalline structure after physical mixing. However, such a peak cannot be found in MCM-41-CUR, suggesting pure curcumin has been loaded successfully in the pores of MCM-41 as nano-sized aggregates.^{23, 24}

Fourier transform infrared (FTIR) analysis was performed to study the interaction between curcumin and MCM-41. To observe the information clearly, only regions of interest are shown in Figure S4. MCM-41 exhibits one typical peak at 3745 cm^{-1} assigned to isolated silanols ($\nu(\text{O-H})$) whereas CUR displays a sharp peak at 3507 cm^{-1} and a broad peak at 3293 cm^{-1} ($-\text{OH}$ group vibrations without and with intermolecular hydrogen bonding, respectively).²⁵ The above three peaks can be observed in the spectrum of MCM-41-CUR PM, however, not in MCM-41-CUR. Instead a new broad peak centered at 3428 cm^{-1} (Fig.S4A) can be seen in MCM-41-CUR due to intermolecular hydrogen bonding between isolated silanol and enolic hydroxyl group²⁶ (Scheme 1B). Additionally, the other typical CUR bands are also found in MCM-41-CUR (Figs. S4A and B).

Solubility of curcumin was determined by preparing saturated solution of CUR, MCM-41-CUR and MCM-41-CUR PM in water to reach the equilibrium concentration. Curcumin solubility was increased by 71% in MCM-41-CUR (0.53 $\mu\text{g}/\text{ml}$) compared to CUR (0.31 $\mu\text{g}/\text{ml}$, Fig. S5A), in accordance with a previous study using Indole-3-butyric acid loaded in MCM-41.²³ MCM-41-CUR PM showed solubility similar to CUR (0.36 $\mu\text{g}/\text{ml}$). The enhanced solubility of curcumin in MCM-41-CUR is attributed to the encapsulation in nanopores based on Ostwald – Freundlich equation where the solubility enhancement is related to particle size.²⁷ This augmented solubility of curcumin from MCM-41-CUR is also observed from in vitro release profile performed in

0.5% Sodium lauryl sulphate (SLS) as the dissolution medium (Fig. S5B). After 1 h, the release for CUR, MCM-41-CUR and MCM-41-CUR PM was 0.25%, 0.67% and 0.29% respectively. The drug release profile increased slowly for MCM-41-CUR reaching 28.5% after 72 h whereas the drug release for CUR and MCM-41-CUR PM was just 8.9% and 9%, respectively. The faster and higher release amount of CUR from MCM-41-CUR should be attributed to the formation of CUR nano-aggregates in the pore channels of MCM-41.

Taking advantage of the improved solubility and in vitro release profile, cell cytotoxicity studies using MTT assay on SCC-25 cell line was conducted in triplicate (See ESI, *In vitro Cytotoxicity Assay and Table S2 for % cell viability with standard deviation*). MCM-41 showed no cytotoxicity even after 72 h confirming earlier reports of silica nanoparticles to be a better drug carrier system.²⁸ MCM-41-CUR treated cells showed dose and time-dependent higher cell cytotoxicity compared to CUR and MCM-41-CUR PM (Fig. 1A). For example, the cell viability from CUR (46%) and MCM-41-CUR (37%) is similar at 45 ppm dose after 24 h but higher than that of MCM-41-CUR PM (67%). Cytotoxicity from CUR reaches almost maximum activity showing no increase in cytotoxicity at 48 and 72 h. On the other hand, the cell viability from MCM-41-CUR decreases with exposure time showing 11% and only 2% at 48 and 72 h, respectively. The superior cytotoxicity of MCM-41-CUR could be attributed to enhanced and sustained release of curcumin from the MCM-41-CUR as demonstrated from the *in vitro* dissolution studies (Fig S5B). Moreover, it was demonstrated that MSNs upto 250 $\mu\text{g}/\text{ml}$ did not affect cell viability when studied in HEK 293 cells.²⁹ As there is no report using curcumin nano-formulation in SCC-25 cell line, we compared our results with studies performed in MCF-7 cell line using curcumin nanospheres or solid lipid nanoparticles and found the cytotoxicity observed in our studies is comparable.^{7, 30}

We further studied the down-regulation of PcG proteins – enhancer of zeste homolog 2 (EzH2) and B lymphoma Mo-MLV insertion region 1 homolog (Bmi-1) by conducting Western blot analysis on SCC-25 cell line (Fig 1B). The glyceraldehyde-3-phosphate dehydrogenase (GAPDH) was used as an internal loading control in the analysis. We observed that CUR and MCM-41-CUR increases activation of caspase-3 through

generation of cleaved caspase-3 resulting in enhanced cell apoptosis. MCM-41-CUR mediated suppression of PcG proteins and protease mediated apoptosis are the key events in SCC-25 cell death. The efficacy of MCM-41-CUR was clearly evident from the dramatic reduction in EzH2 level compared to CUR. This higher efficacy could be due to the enhanced endocytosis as observed from the higher silica content in SCC-25 cells carrying curcumin cargo in the cells (Fig. S6) and time-dependent controlled release of curcumin from MCM-41-CUR. Though there are not many reports focusing on the impact of curcumin nano-formulation on PcG proteins, our observation is in line with previous report studying the effect of free curcumin on down-regulation of EzH2 expression in human breast cancer MDA-MB-435 cells.³¹

In summary, we have demonstrated a simple and efficient technique for curcumin encapsulation in the nanopores of MCM-41 type MSNs. This strategy leads to improved aqueous solubility, enhanced drug release, and high cellular delivery efficiency of curcumin. Consequently, compared to the pure drug, curcumin encapsulated in MCM-41 possesses enhanced cytotoxic effect, which is linked with the inhibition of PcG proteins and activation of caspase-3. This work provides a simple but efficient method to design new curcumin based nano-formulations to improve its therapeutic efficacy.

We thank the Australian Research Council and Cancer Council of Queensland for financial support. We acknowledge the Australian National Fabrication Facility and the Australian Microscopy and Microanalysis Research Facility at the Centre for Microscopy and Microanalysis, the University of Queensland.

^a Australian Institute for Bioengineering and Nanotechnology, The University of Queensland, Brisbane, QLD 4072, Australia. Fax: +61 7 3346 3973; Tel: +61 7 3346 3283; E-mail: c.yu@uq.edu.au

‡ These authors contribute equally to this paper

† Electronic Supplementary Information (ESI) available: Experimental details and Results. See DOI: 10.1039/b000000x/

Notes and references

1. M. T. Huang, Y. R. Lou, W. Ma, H. L. Newmark, K. R. Reuhl and A. H. Conney, *Cancer Res*, 1994, **54**, 5841-5847.
2. A. Duvoix, R. Blasius, S. Delhalle, M. Schnekenburger, F. Morceau, E. Henry, M. Dicato and M. Diederich, *Cancer Lett*, 2005, **223**, 181-190.
3. P. Anand, C. Sundaram, S. Jhurani, A. B. Kunnumakkara and B. B. Aggarwal, *Cancer Lett*, 2008, **267**, 133-164.
4. S. Shishodia, G. Sethi and B. B. Aggarwal, in *Natural Products and Molecular Therapy*, eds. G. J. Kotwal and D. K. Lahiri, New York Acad Sciences, New York, 2005, vol. 1056, pp. 206-217.
5. M. M. Yallapu, M. Jaggi and S. C. Chauhan, *Curr Pharm Design*, 2013, **19**, 1994-2010.
6. P. Couvreur, C. Dubernet and F. Puisieux, *Eur J Pharm Biopharm*, 1995, **41**, 2-13.
7. R. S. Mulik, J. Monkkonen, R. O. Juvonen, K. R. Mahadik and A. R. Paradkar, *Int J Pharm*, 2010, **398**, 190-203.
8. C. Oussoren and G. Storm, *Adv Drug Deliver Rev*, 2001, **50**, 143-156.
9. M. Vallet-Regi, A. Ramila, R. P. del Real and J. Perez-Pariante, *Chem Mater*, 2001, **13**, 308-311.
10. D. Tarn, C. E. Ashley, M. Xue, E. C. Carnes, J. I. Zink and C. J. Brinker, *Accounts Chem Res*, 2013, **46**, 792-801.

11. A. Szegeedi, M. Popova, I. Goshev and J. Mihalý, *J Solid State Chem*, 2011, **184**, 1201-1207.
12. N. W. Clifford, K. S. Iyer and C. L. Raston, *J Mater Chem*, 2008, **18**, 162-165.
13. Y. L. Choi, J. Jaworski, M. L. Seo, S. J. Lee and J. H. Jung, *J Mater Chem*, 2011, **21**, 7882-7885.
14. D. Jin, K. W. Park, J. H. Lee, K. Song, J. G. Kim, M. L. Seo and J. H. Jung, *J Mater Chem*, 2011, **21**, 3641-3645.
15. Y. J. Wang, M. H. Pan, A. L. Cheng, L. I. Lin, Y. S. Ho, C. Y. Hsieh and J. K. Lin, *J Pharmaceut Biomed*, 1997, **15**, 1867-1876.
16. T. Niidome, M. Yamagata, Y. Okamoto, Y. Akiyama, H. Takahashi, T. Kawano, Y. Katayama and Y. Niidome, *J Control Release*, 2006, **114**, 343-347.
17. Q. J. He, J. L. Shi, F. Chen, M. Zhu and L. X. Zhang, *Biomaterials*, 2010, **31**, 3335-3346.
18. S. Liu, M. S. Wolfe and R. T. Borchardt, *Antivir Res*, 1992, **19**, 247-265.
19. K. Lee, G. Adhikary, S. Balasubramanian, R. Gopalakrishnan, T. McCormick, G. P. Dimri, R. L. Eckert and E. A. Rorke, *J Invest Dermatol*, 2008, **128**, 9-17.
20. Z. S. Xu, H. T. Liu, X. Q. Lv, Y. Q. Liu, S. L. Li and H. X. Li, *Oncol Rep*, 2011, **25**, 409-418.
21. C. T. Kresge, M. E. Leonowicz, W. J. Roth, J. C. Vartuli and J. S. Beck, *Nature*, 1992, **359**, 710-712.
22. T. Limmell, H. A. Santos, E. Makila, T. Heikkila, J. Salonen, D. Y. Murzin, N. Kumar, T. Laaksonen, L. Peltonen and J. Hirvonen, *J. Pharm. Sci.*, 2011, **100**, 3294-3306.
23. V. Ambrogio, F. Famiani, L. Perioli, F. Marmottini, I. Di Cunzolo and C. Rossi, *Micropor Mesopor Mat.*, 2006, **96**, 177-183.
24. M. Vialpando, A. Aerts, J. Persoons, J. Martens and G. Van den Mooter, *J. Pharm. Sci.*, 2011, **100**, 3411-3420.
25. T. M. Kolev, E. A. Velcheva, B. A. Stamboliyska and M. Spittler, *Int J Quantum Che*, 2005, **102**, 1069-1079.
26. R. K. Gangwar, V. A. Dhumale, D. Kumari, U. T. Nakate, S. W. Gosavi, R. B. Sharma, S. N. Kale and S. Datar, *Mater Sci Eng C Mater Biol Appl*, 2012, **32**, 2659-2663.
27. W. Ostwald, *Z Phys Che-Stoch Ve*, 1900, **34**, 495-503.
28. J. Lu, M. Liong, Z. X. Li, J. I. Zink and F. Tamanoi, *Small*, 2010, **6**, 1794-1805.
29. R. Guillet-Nicolas, A. Popat, J. L. Bridot, G. Monteith, S. Z. Qiao and F. Kleitz, *Angew Chem Int Edit*, 2013, **52**, 2318-2322.
30. N. Suwannateep, W. Banlunara, S. P. Wanichwecharungruang, K. Chiablaem, K. Lirdprapamongkol and J. Svasti, *J Control Release*, 2011, **151**, 176-182.
31. W. F. Hua, Y. S. Fu, Y. J. Liao, W. J. Xia, Y. C. Chen, Y. X. Zeng, H. F. Kung and D. Xie, *Eur J Pharmacol*, 2010, **637**, 16-21.